Available online at www.sciencedirect.com
SCIENCE DIRECT
Geochimica et Cosmochimica Acta 70 (2006) 3803–3819
Geochimica
www.elsevier.com/locate/gca

Interactions of biopolymers with silica surfaces: Force measurements and electronic structure calculation studies

Kideok D. Kwon [a,*], Virginia Vadillo-Rodriguez [b], Bruce E. Logan [b], James D. Kubicki [a,c]

[a] Department of Geosciences, The Pennsylvania State University, University Park, PA 16802, USA
[b] Department of Civil and Environmental Engineering, The Pennsylvania State University, University Park, PA 16802, USA
[c] Earth and Environmental Systems Institute, The Pennsylvania State University, University Park, PA 16802, USA

Received 1 January 2006; accepted in revised form 31 May 2006

Abstract

Pull-off forces were measured between a silica colloid attached to an atomic force microscope (AFM) cantilever and three homopolymer surfaces representing constituents of extracellular polymeric substances (EPS). The pull-off forces were −0.84 (±0.16), −0.68 (±0.15), and −2.37 (±0.31) nN as measured in water for dextran, phosphorylated dextran, and poly-L-lysine, respectively. Molecular orbital and density functional theory methods (DFT) were applied to analyze the measured pull-off forces using dimer clusters representing interactions between the three polymers and silica surfaces. Binding energies for each dimer were calculated with basis set superposition error (BSSE) and interpolated using corrections for silica surface hydroxyl density and silica charge density. The binding energies were compared with the normalized pull-off forces with the effective silica surface area contacting the polymer surfaces. The predicted binding energies at a $-0.064\ C/m^2$ silica surface charge density corresponding to circum-neutral pH were −0.055, −0.029, and $-0.338 \times 10^{-18}\ J/nm^2$ for the dimers corresponding to the silica surface with dextran, phosphorylated dextran, and poly-L-lysine, respectively. Polarizable continuum model (PCM) calculations with different solvents, silanol vibrational frequency calculations, and orbital interaction analysis based on natural bonding orbital (NBO) showed that phosphate groups formed stronger H-bonds with neutral silanols than hydroxyl and amino functional groups of polymers, implying that phosphate containing polymers would play important roles in EPS binding to silica surfaces.

1. Introduction

Microbial extracellular polymeric substances (EPS) are a complex mixture of biopolymers such as polysaccharides, proteins, nucleic acids, and lipids around the microbial cell surface (Wingender et al., 1999). In nature, EPS are often associated with mineral surfaces and are important in processes such as mineral dissolution (Welch et al., 1999), biomineralization (Chan et al., 2004), sediment stabilization (Dade et al., 1990), bacterial adhesion (Marshall et al., 1989; Fletcher, 1996), biofilm formation (Costerton et al., 1985; Vandevivere and Kirchman, 1993; Becker, 1996), and pollutant distribution (Wolfaardt et al., 1994; Loaëc et al., 1997).

Among EPS constituents, extracellular nucleic acids have been relatively ignored in EPS interactions with mineral surfaces because of the minor composition in EPS (Wingender et al., 1999). Polysaccharides and proteins are dominant components of EPS (Wolfaardt et al., 1999), hence extracellular polysaccharides and proteins have been regarded as major biopolymers in controlling the interactions with mineral surfaces. Recent studies, however, have shown extracellular nucleic acids as an important component of EPS in biofilm formation (Whitchurch et al., 2002) and bacterial adhesion to mineral surfaces (Omoike et al., 2004; Omoike and Chorover, 2006). Therefore, comparison of the interactions of each EPS component (e.g., nucleic acids, polysaccharides, and proteins)

* Corresponding author. Fax: +1 814 863 7823.
E-mail address: kkwon@geosc.psu.edu (K.D. Kwon).

0016-7037/$ - see front matter © 2006 Elsevier Inc. All rights reserved.
doi:10.1016/j.gca.2006.05.016

with mineral surfaces would be necessary to understand the roles of and contributions of each type of compound to the complex interactions with mineral surfaces.

In this current study, interactions of three different polymers with silica surface were investigated in order to deduce the nature of the different interactions (e.g., interaction strength and the dominant interaction forces) of EPS components with specific mineral surfaces. Homopolymers (e.g., a polymer consisting of one repeating unit) such as dextran, phosphorylated dextran, and poly-L-lysine were used as analogues to represent EPS components. Silica was selected because silica is one of the most abundant minerals in subsurface environments. Relative binding strengths and interacting force types of the polymers with silica surfaces were determined by molecular level approaches.

Atomic force microscopy (AFM) (see Cappella and Dietler, 1999 for review) has been used as a tool to provide force information of polymer interactions with surfaces. Various AFM studies have shown direct measurements of the interaction forces of functional groups, biopolymers, EPS, and bacteria with surfaces by modifying AFM tips or substrate surfaces (Lower et al., 2000; van der Aa and Dufrene, 2002; Kendall and Hochella, 2003; Kreller et al., 2003). Thus, in this study, to determine the relative binding strengths of the polymers, pull-off forces (i.e., force corresponding to a maximum jump-off-contact deflection of a cantilever in a withdrawal curve) of the polymers covalently attached to a slide glass (i.e., SAM) were measured with a colloidal silica bead attached to an AFM cantilever. Two different media, distilled water and perfluorodecalin (PFD, $C_{10}F_{18}$), were used to study solvent effects on the interactions between polymers and surfaces. PFD has been known to enhance differences in pull-off forces of various polymers due to the low dielectric constants (1.86) (Feldmann et al., 1998). A low dielectric constant medium is desirable because it mimics the gas-phase calculations and serves as a contrast to the strong solvent interactions present in the water experiments.

Molecular modeling can provide detailed structural and energetic information between adsorbates and surfaces, whereas short-range (<1 nm) chemical and physical characteristics of interacting polymers with an AFM tip are generally not well resolved in AFM studies (Ashby et al., 2000). Previously, classical molecular dynamics (MD) simulations have been applied to help interpret AFM studies (Grubmüller et al., 1996; Konrad and Bolonick, 1996; Izrailev et al., 1997; Harrison et al., 1999). Recent MD simulations tested detailed geometries of interactions between self-assembled monolayers (SAM) (Ulman, 1996) attached to an AFM tip and substrates on an experimental time scale (Leng and Jiang, 2002). However, few studies have been conducted to investigate interactions between polymers and bare mineral surfaces. One such study was performed by Kendall et al. (2005) who applied MD simulations to organic ligands interactions with mineral surfaces. The scarcity of this type of study is due to the difficulty in obtaining accurate force fields that describe the polymer-surface interactions.

As an alternative approach, quantum mechanical calculations can be used to predict chemical properties of the interactions because a force field is not necessary. However, the limitation of quantum mechanical methods is that they typically cannot be applied to large systems and incorporate the dynamic force process as in classical MD simulations. Thus, although our modeling efforts neglect the larger scale aspects of polymer-surface interactions and the dynamic behavior, we attempt to connect AFM force measurements with molecular-scale processes by determining the relative binding strength between monomers of each polymer type and a small model of the silica colloid AFM tip used in this study.

In electronic structure calculations, interaction potential energies between the polymers and silica surface were estimated to compare to measured pull-off forces. Measured pull-off forces, however, are dynamic quantities because measured bond strengths depend on force loading rate (Evans and Ritchie, 1997; Merkel et al., 1999). The external force lowers energy barriers and can significantly increase the bond dissociation rates (Evans, 2001). Therefore, direct quantitative comparison of calculated thermodynamic information of molecular interactions with the measured forces is limited. However, the relative strength of the three polymers measured at one loading rate can be rationalized as a thermodynamic quantity, because the relative strength is originated from the difference in their chemical interactions toward silica surfaces.

The pull-off forces of homopolymers measured for a short time-interval can be regarded as multiples of a single type of interaction between a repeating unit of polymers and a unit area of silica surface, assuming that the measured force is a sum of individual interactions between the AFM tip and substrates (Hoh et al., 1992; Florin et al., 1994). Adhesion forces measured in AFM experiments have a linear correlation with the binding enthalpy rather than the free energy of a system (Moy et al., 1994; Chilkoti et al., 1995). Therefore, monomeric repeating units of polymers and silica surfaces were modeled to represent parts of the interactions between the polymers and the silica colloid, and the binding energy of each model dimer (i.e., enthalpy required to separate an interacting dimer into two isolated monomers) was calculated to analyze the measured forces, which were normalized with the contact area of silica surface with polymers. Solvent continuum models with different dielectric constants (Klamt and Schuurmann, 1993) were used to analyze the force differences measured in water and in PFD. Lastly, the interactions of model dimers were investigated with silanol vibrational frequency and orbital interaction analyses. These analyses are useful for understanding relative interaction strengths in terms of H-bonding and for interpreting vibrational spectra of the adsorbed monomers.

2. Materials and methods

2.1. Force measurements

Self-assembled monolayer (SAM) polymer surfaces and a silica colloid were used in the force measurements in an effort to minimize the contact geometry change of silica surface with polymers and to better constrain the polymer locations. The polymers tethered to glass would limit peel-off of the polymers from the glass surface during force measurements. Approximately 10 nm thick SAMs of poly-L-lysine (M_w ca. 10 kDa) and dextran (M_w ca. 10 kDa) (XanTec bioanalystics, Germany), which were covalently bonded to silanes of the slide glass based on amide bonds (Frey and Corn, 1996), were used as substrates in the measurements. Phosphorylated dextran surfaces (XanTec bioanalystics, Germany) were prepared by attaching phosphates to dextran already coated to a glass surface (averaged phosphate density is below one per D-glucose unit).

The AFM probes were V-shaped silicon nitride cantilevers with a ca. 1 μm SiO_2 particle attached (Novascan Technology, Ames, IA) (Fig. 1a). The spring constant of the colloidal tips was 0.152 (±0.004) N/m, which was determined with the thermal tuning method (Nanoscope V6.12r2).

Force measurements were conducted using a Bioscope AFM (Digital Instruments, CA) with a NanoScope IIIa control system. Milli-Q water (ca. pH 5, not buffered) was added and left for ca. 10 min before collecting force–distance curves. Perfluorodecalin (Aldrich) was used as a contrasting, low dielectric constant medium in parallel measurements. The force curves were obtained at 1 Hz of z-scan rate, 1.5 μm z-scan size, and 100 nm maximum deflection from 18 to 26 different random positions of each surface by moving the microscope stage.

Although the external parameters were kept constant during the measurements, the standard deviation of the measured force from the averaged value was up to 20%. However, the limited reproducibility did not affect the determination of the relative bond strength of polymers in the study. Distributions of the pull-off forces were plotted as histograms with a bin size of 0.04–0.5 nN. The pull-off forces were normalized with the contact areas of the silica colloid to compare with calculated binding energies by the general relationship of force and energy between a sphere and a flat surface (i.e., $F/2\pi a$) gives energy per area unit, J/m^2, where F is a mean pull-off force, and a is a contacting radius of a silica sphere on polymer surfaces; (Israelachvili, 1991).

Areas of an AFM tip contacting with polymer surfaces are determined by several parameters such as tip contact time and tip loading force. In this study, contact areas of the silica colloidal tips were estimated by calculating contacting radius (a) of a sphere with flat surface based on modified Johnson, Kendall, and Roberts (JKR) model (Johnson et al., 1971) mainly assuming pure elastic deformation and paraboloid curvature of the sphere,

$$a = \left(\frac{R}{K}\right)^{1/3}\left(\sqrt{-F_c^{\mathrm{JKR}}} + \sqrt{F_l - F_C^{\mathrm{JKR}}}\right)^{2/3} \quad (1)$$

where R is the colloidal sphere radius, F_c^{JKR} is the measured force to separate the sphere from the surface (pull-off forces here), F_l is the externally applied loading force (maximum

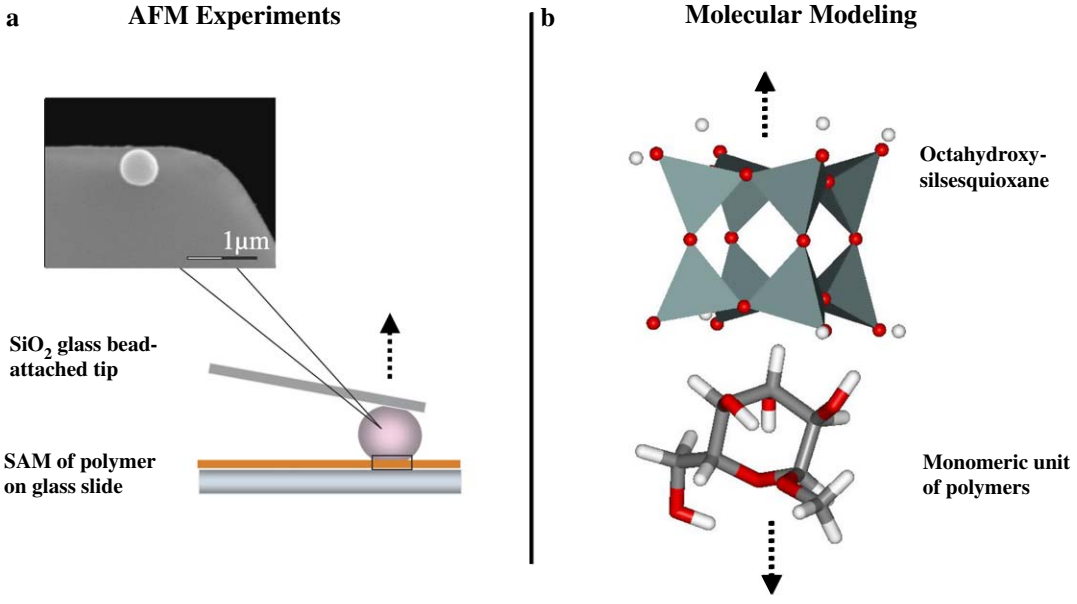

Fig. 1. Schematic description of (a) conducted AFM experiments with the SEM image of a 1 micron SiO_2 colloid attached to a Si_3N_4 cantilever and (b) models used in electronic structure calculations to represent the interactions between polymers and silica surface (the rectangular area in (a)). The pull-off forces measured in experiments were compared to the binding energies of models in molecular modeling (see arrows). Gray tetrahedra, SiO_4; Red, oxygen; White, hydrogen; Grey, carbon atom. The molecular models were drawn using ViewerLite (Accelrys Inc., CA), a molecular visualization program. (For interpretation of the references to color in this figure legend, the reader is referred to the web version of this paper.)

deflection points in approaching curves here), and K represents the effective elastic modulus by $4/3[(1-\nu_1^2)/\varepsilon_1+(1-\nu_2^2)/\varepsilon_2]^{-1}$ (ε, the elastic modulus; ν, the Poisson's ratio) (see Schwarz, 2003 for detailed linear-elastic mechanical models). The elastic modulus and the Poisson's ratio of silica glass ($\varepsilon = 72.9$ GPa and $\nu = 0.165$ at 23 °C Spinner, 1956) were used in the Eq. (1) by assuming that the ε and ν of thin-polymer coated glass are not much different from those of the silica colloidal particles. A recent MD simulation study has shown the limitations of current linear-elastic mechanics models, but the simulated contact radii of SAM on a flat surface were better agreement with the JKR model than other linear-elastic models (Patrick et al., 2003).

2.2. Computational details

2.2.1. Model structures

A double-four-membered ring of $SiO_2(Si_8O_{12}(OH)_8$, octa-hydroxy silsesquioxane, OHS) (Marcolli and Calzaferri, 1999) was used to represent a silica surface structure (Fig. 1b). OHS has a stable structure and the prominent functional groups of silica surfaces (i.e., silanols and siloxanes). Monomeric units of the polymers were modeled to represent the biopolymers interacting with a silica colloidal tip in the AFM force measurements: a methyl glucoside ($C_6H_{11}O_6(CH_3)$, DET) capturing a glycoside bond of dextran (Fig. 2a); a methyl glucosidic phosphate ($C_6H_{10}O_5(CH_3)(HPO_4^-)$, PHO) for phosphorylated dextran (Fig. 2b); a lysine peptide unit ($NH_3^+(CH_2)_4CH_2CONHCH_3$, LYS) for polylysine (Fig. 2c).

The monomeric units were modeled to take the appropriate charges in the experimental pH. Dextran is a neutral polysaccharide. Phosphorylated dextran and polylysine would take approximately (−1) negative and (+1) positive charges per monomer in the pH range 5–7 in aqueous solution because the pK_as of the phosphate and lysine are kwon as ca. 1 and 6 and ca. 11, respectively. The isoelectric point of charge of silica (2–4 Parks, 1965) and recent XPS and thermodynamic model study of quartz (Duval et al., 2002) suggest major surface groups on silica surface would be ≡Si—OH with minor ≡Si—O^- in the neutral to slightly acidic pH range. Therefore, binding energies of monomeric units with OHS were calculated using neutral charged OHS as well as (−1) charged OHS ($^-$OHS).

2.2.2. Energy minimizations of model structures

Gaussian 03 (Frisch et al., 2003) was used in all molecular orbital calculations of the model structures. Each monomer and dimer structure (i.e., DET/OHS, PHO/OHS, and LYS/OHS) were fully energy-minimized in a gas phase using Hartree-Fock (HF) with the 3-21G(d,p) basis set (Gordon et al., 1982) without any constraints. Computational accuracy such as H-bond distances can be improved, in principle, by using larger basis sets and

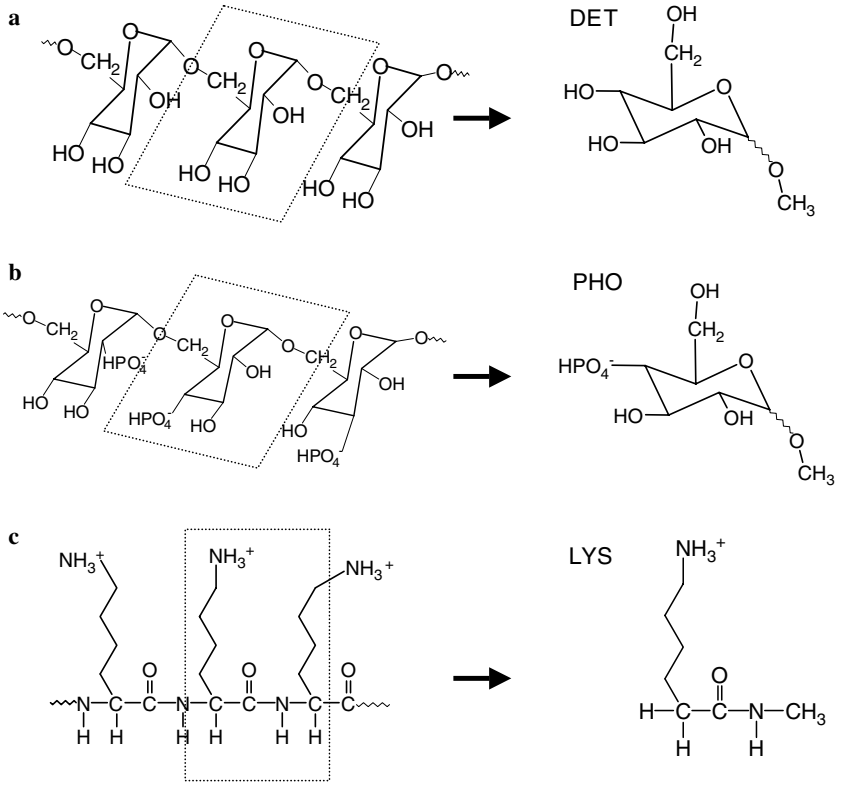

Fig. 2. Model structures of monomeric units of polymers interacting with octahydroxy silsesquioxane (OHS): (a) dextran and its monomeric model unit (DET), (b) phosphorylated dextran and its monomeric model unit (PHO), and (c) poly-L-lysine and its monomeric model unit (LYS).

post-HF methods. Tests showed that the HF method had a tendency to overestimate H-bond distances of dimers compared to B3LYP functionals (Lee et al., 1988; Becke, 1993) based on the 3-21G(d, p) basis set.

Previous IR studies have suggested that the main interaction types with silica surfaces are H-bonds and/or electrostatic interactions for phosphates in nucleic acids (Mercier and Savoie, 1997) and hydroxyl groups in dextran (Jucker et al., 1997). For poly-L-lysine, amine groups have been suggested as important for adsorption onto TiO_2 (Roddick-Lanzilotta and McQuillan, 1999). Consequently, dimer initial structures were created to maximize the interactions through H-bonds and favorable electrostatic interactions between OHS and functional groups of the monomeric units.

For the energy-minimization of each monomer, detailed conformers of monomer itself were not explored. Instead, an effort was made to minimize intramolecular interactions on the monomeric units themselves. Energy minimization in the gas phase can overestimate intramolecular interactions of a molecule, and the overestimations can make it more complicated to find optimal intermolecular interactions (e.g., H-bonds) between dimers. For example, LYS, which has the flexible alkyl chain, can take a bent structure due to strong intramolecular interactions of a NH_3^+ with a C=O of the peptide bond (—CONH—) in a gas-phase energy minimization. The bent LYS configuration does not lead to optimal intermolecular interactions of the NH_3^+ and the peptide bond with silanols groups of OHS. The energy variation of the energy-minimized monomeric unit conformers was approximately 3–5 kJ/mol, which did not affect the current interpretation in this study.

2.2.3. Binding energy calculations of model structures

Binding energies (ΔH_{bind}) of dimers (i.e., the required enthalpy to disassemble the dimer into each monomer, $AB \rightarrow A + B$), were calculated by

$$\Delta H_{bind} = -(H_{MON} + H_{OHS} - {}^{*}H_{MON/OHS}) - E_{DEF} \quad (2)$$

where H_{MON} and H_{OHS} are the estimated enthalpies of fully optimized monomeric units and OHS, and ${}^{*}H_{MON/OHS}$ is the estimated enthalpy of a fully energy-minimized dimer with basis set superposition error (BSSE, an artificial lowering of a dimer energy) correction. The BSSE becomes significant when two monomers come closer to each other in a dimer, especially when using a small basis set such as 3-21G(d, p). Deformation energy (E_{DEF}) is a repulsion energy caused by deformation of monomer structures upon formation of dimers (Hobza and Sponer, 1999). The deformation energy was calculated by the electronic energy difference between the monomers in optimized dimer geometries and the isolated monomers (i.e., $E_{DEF} = (E_{MON\_dimer} - E_{MON}) + (E_{OHS\_dimer} - E_{OHS})$, where E_{MON_dimer} and E_{OHS_dimer} are the electronic energies of a monomeric unit and an OHS, respectively, in the dimer geometry). Due to the negative sign in Eq. (2), a more negative ΔH_{bind} means stronger binding energy between monomers and corresponds to stronger pull-off forces in the AFM experiments.

The potential energies of model structures and BSSE were calculated by single-point energy calculations using B3LYP functionals with the 6-311++G(d, p) basis set (Hehre et al., 1972) based on the energy-minimized structures obtained with the HF/3-21G(d, p) method. The larger polarized-valence, triple-zeta basis set (6-311G(d, p)) reduces BSSE and more accurately predicts interactions in H-bonded dimers (Paizs and Suhai, 1998). Inclusion of diffuse functions (++) in a basis set is important in the hybrid density functional theory (DFT) such as B3LYP to obtain relative energies of molecules (Lynch et al., 2003) and to reduce BSSE in H-bond interactions of carbohydrates (Lii et al., 1999). The counterpoise method (Boys and Bernardi, 2002) was used to estimate the BSSE evolved in binding calculations and to estimate inadequacy of limited basis sets (Schwenke and Truhlar, 1985; Frisch et al., 1986) with the B3LYP/6-311++G(d,p) method. A test with a same LYS/OHS structure confirmed that B3LYP with the extensive basis set significantly reduce BSSE (17 kJ/mol) compared to the HF/3-21G(d, p) method (70 kJ/mol).

Enthalpies of the model structures were estimated by harmonic vibration analysis to obtain zero-point energy and thermal energy contributions based on statistical thermodynamics. Because the energy minimization and frequency calculations with a large 6-311++G(d, p) basis set is not practical within our computing capacity, the zero-point energy and thermal energy correction at 298 K and 1 atm were calculated using HF/3-21G(d, p).

2.2.4. IR vibrational frequencies and natural bond orbital (NBO) analysis

Red-shifting of silanol O—H stretching vibrational frequency and the increase of the IR intensity proportional to the change of the dipole moments can be used as a measure of H-bond strength (Jeffrey, 1997). The vibrational frequencies of OHS silanols and the IR intensities were calculated with HF/3-21G(d, p) based on the energy-minimized geometries with the same method. The calculated frequencies were reported without scaling the frequency overestimation caused by the use of harmonic oscillation assumption, incomplete basis sets and the neglect of electron correlation.

H-bonds of polymer units with neutral OHS were analyzed with interactions between filled and unfilled orbitals (e.g., charge transfer, $n \rightarrow \sigma^*$, where n is lone pair electrons, and σ^* is an unfilled antibonding orbital) (Reed et al., 1986, 1988; Bach et al., 2001; Vorobyov et al., 2002) based on the localized Natural Bond Orbitals (Reed and Weinhold, 1985). Such orbital interactions are known to lower the molecular energy via the electron delocalization. The electron populations and the stabilizing energies were calculated with the 2nd perturbation analysis in the Natural Bond Orbital (NBO) 3.1 program (Reed et al., 1988) based on B3LYP/6-311++G(d, p) canonical orbitals.

2.2.5. Solvent effects on binding energy

The binding energies of polymer units with neutral OHS in different solvents (e.g., water, ethanol, and heptane) were estimated with one of models treating the solvent as a continuum, the conductor-like polarizable continuum (C-PCM) model (Klamt and Schuurmann, 1993; Cossi et al., 2003). The continuum model treats solvent effects by incorporating polarizations between a solute wave function and solvent potentials through parameters such as dielectric constants (see Tomasi and Persico, 1994; Cramer and Truhlar, 1999 for details). Solvation energy (ΔG_{sol}) in the continuum model accounts for the polarization between a solute and a solvent (i.e., electrostatic interactions) and non-electrostatic interactions (e.g., work needed to make cavity around a solute). The solvation energy is intrinsically a free energy, and enthalpy has not been clearly defined in this type calculation. In this study, the difference of explicit summation of E (internal energy in a continuum cavity) and its ΔG_{sol} between a dimer and monomers (i.e., $\Delta(E+\Delta G_{sol})$) was used to represent the interaction strength. The energies with different solvents were calculated with B3LYP/6-311++G(d, p) based on the energy-minimized structures in the gas phase without BSSE and enthalpy corrections. The united atom model optimized for HF/6-31G(d) level (UAHF) (Barone et al., 1997) was used for the solvent radii.

2.2.6. Potential energy curves and force curves

A simple rigid-body approximation is typically used in predicting the potential energy curves of even flexible molecules, because incorporation of the intramolecular interactions into potential energy surface of intermolecular interaction is complicated (Stone, 1996; Chalasiński and Szczęśniak, 2000). However, the approximation often prevents finding maximized intermolecular interactions and predicts similar harmonic-style potential wells of dimers around the potential minima. The similar curvatures of the potential curves produce similar derivatives (e.g., force curves) for dimers despite significant differences in the potential energy minima. Hence, more degrees of freedom can be allowed in the geometry optimization of dimers to obtain more realistic geometries and interacting forces (e.g., interacting functional groups are relaxed between a dimer).

The LYS/OHS dimer was repeatedly energy-minimized at fixed distances between the monomers as a function of the distance to obtain the potential energy curve. The dimer was gradually taken apart and put together at approximately 0.5 Å step size starting from the fully energy-minimized dimer structure. Around the minima of potential energy curves, a smaller step size (0.1 Å) was used. The distance was determined between a selected carbon atom of LYS that was not directly interacting with silanols of OHS and a dummy atom on the OHS obtained by normal projection of the reference atom to the upper 4 Si-atom plane of OHS.

During the energy minimizations at fixed distances, geometry constraints were imposed to keep the distance of the dimer constant and to see the effect of the number of degrees of freedom in geometry on the resulting forces. The coordinates of six, four, and three carbon atoms of LYS including reference atoms were fixed at corresponding distances, but the remaining atoms of LYS were relaxed. Atom positions of OHS were kept constant except the interacting parts of OHS (i.e., hydroxyl groups) with LYS.

Interaction forces between the LYS/OHS dimer, $F(x)$, were obtained from the force and potential relationship in a conservative system

$$F(x) = -\frac{dU(x)}{dx} \tag{3}$$

where x is a distance between two molecules, and $U(x)$is the potential energy of the dimer at x. The potential energy, $U(x)$, was obtained by polynomial fitting of the interaction energies of dimers calculated with B3LYP/6-311++G(d, p) using Matlab 6.5 (Mathworks Inc., Natick, MA). The force, $F(x)$, was calculated by the analytical derivative of the fitted potential.

3. Results

3.1. Measured pull-off force and converted interaction energy

The pull-off forces of the three polymers measured in PFD solvent were greater by approximately one order of magnitude than those measured in H_2O (Fig. 3). The pull-off forces of poly-L-lysine with a silica colloid particle tip were higher than those of the other two polymers in both solvents (Fig. 3c and f). The mean pull-off force (F_{mean}) of phosphorylated dextran was similar to F_{mean} of dextran in water but much higher than F_{mean} of dextran and almost same as F_{mean} of poly-L-lysine in PFD (Table 1). The F_{mean} of dextran, phosphorylated dextran, and poly-L-lysine were −0.84, −0.68, and −2.37 nN in water and −5.44, −11.82, and −12.36 nN in PFD, respectively. The contact radii of the silica spheres with the polymer surfaces estimated with Eq. (1) were 5–6 nm in H_2O and 7–9 nm in PFD solvent (Table 1). Based on the contact area of the tip, the normalized interaction energies of the mean pull-off forces were estimated in a same strength order to F_{mean} as −0.026, −0.022, and -0.061×10^{-18} J/nm^2 in H_2O and −0.122, −0.220, and -0.231×10^{-18} J/nm^2 in PFD for dextran, phosphorylated dextran, and poly-L-lysine surface, respectively.

3.2. Energy-minimized structures and binding energies

3.2.1. DET with OHS

Two possible configurations were tested in binding directions of DET to the OHS surface. One was a parallel binding of the DET ring to the OHS surface. The other was a vertical binding in a manner such that the methyl and hydroxymethyl groups did not interact with OHS surface, and three hydroxyl groups of the ring form H-bonds with silanols of OHS. (A H-bond is defined here as a bond

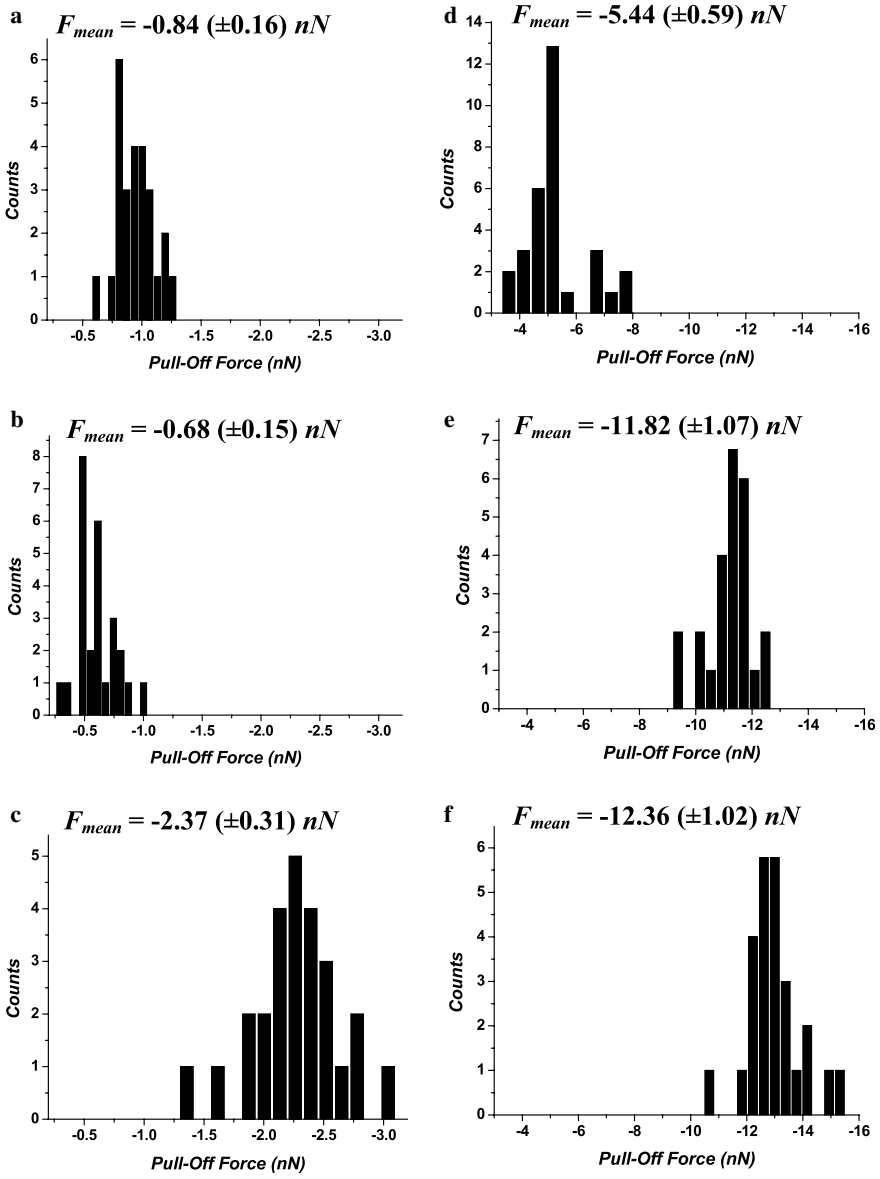

Fig. 3. Histograms of the pull-off forces of polymers measured with a silica probe: (a) dextran in water, (b) phosphorylated dextran in water, (c) poly-L-lysine in water, (d) dextran in perfluorodecalin, (e) phosphorylated dextran in perfluorodecalin, (f) poly-L-lysine in perfluorodecalin.

Table 1
Measured pull-off forces of polymers with a a-SiO_2 colloidal tip in H_2O and PFD (perfluorodecalin) media and their normalized values (pull-off energy) with the contact radii

	Pull-off force[a] (nN)		Pull-off energy[b] (10^{-18} J/nm^2)		Contact radius[c] (nm)	
	H_2O	PFD	H_2O	PFD	H_2O	PFD
Dextran	−0.84 (±0.16)	−5.44 (±0.59)	−0.026 (±0.005)	−0.122 (±0.010)	5.1 (±0.1)	7.1 (±0.2)
Phosphorylated dextran	−0.68 (±0.15)	−11.82 (±1.07)	−0.022 (±0.004)	−0.220 (±0.014)	4.8 (±0.2)	8.5 (±0.2)
Poly-L-lysine	−2.37 (±0.31)	−12.36 (±1.02)	−0.061 (±0.007)	−0.231 (±0.014)	6.2 (±0.2)	8.5 (±0.2)

Reported values are mean values with their standard deviations in parentheses.
[a] Mean pull-off forces.
[b] Normalized energy of the pull-off force using $F/2\pi a$ (F, pull-off force; a, contacting radius[c]).
[c] Radius of a silica sphere contacting with polymer surfaces obtained by the JKR model.

between an electron-deficient hydrogen and a region of high electron density.) Because the latter case had lower energy than the former configuration by approximately 10 kJ/mol, we used the lower energy configuration for subsequent calculations (Fig. 4a). When extension of the monomeric unit to a polymer is considered, the vertical

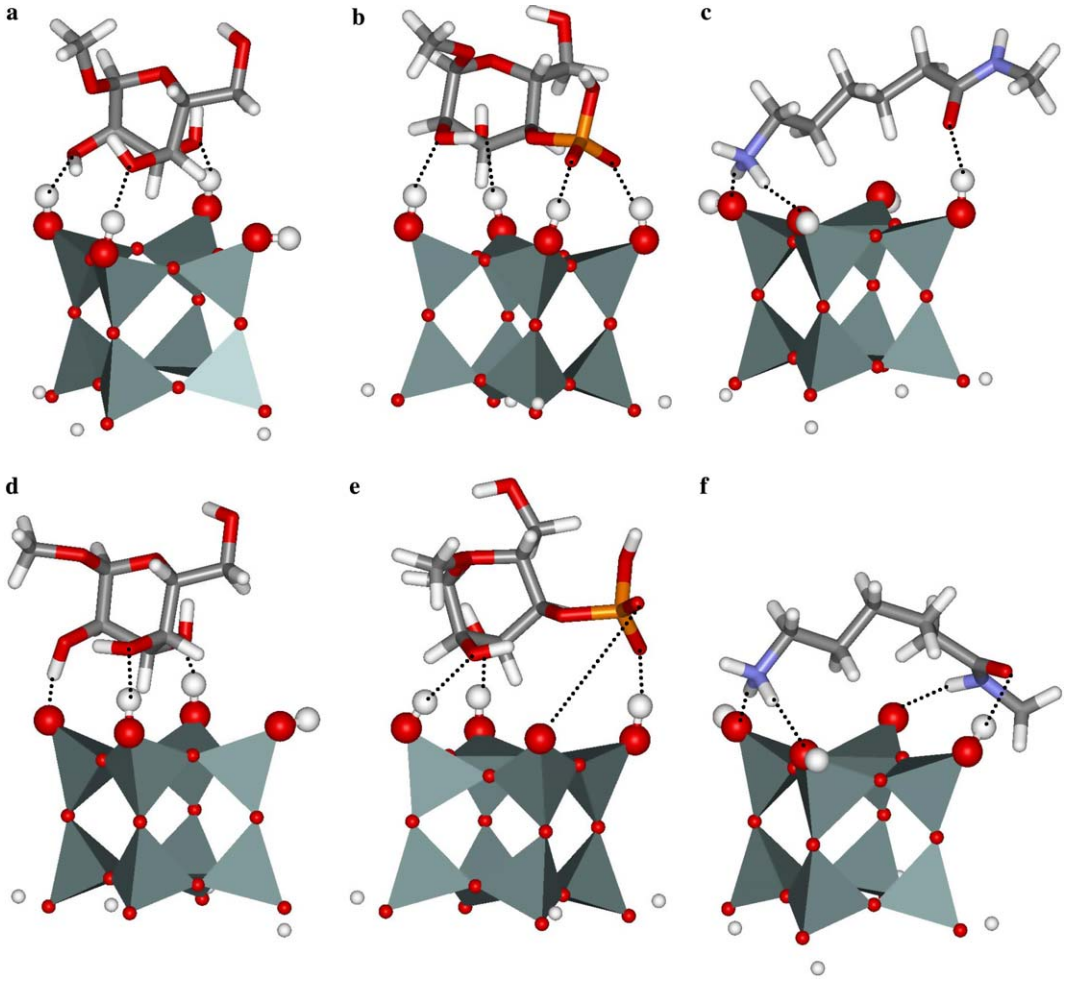

Fig. 4. Fully energy-minimized model structures interacting with neutral OHS and negatively charged OHS ($^{-}$OHS): (a) DET/OHS, (b) PHO/OHS, (c) LYS/OHS, (d) DET/$^{-}$OHS, (e) PHO/$^{-}$OHS, and (f) LYS/$^{-}$OHS. Dotted lines represent H-bonds and guide corresponding interactions of the dimers. Gray tetrahedra, SiO_4; Red, oxygen; Blue, nitrogen; Orange, phosphorus; White, hydrogen; Grey, carbon atom. (For interpretation of the references to color in this figure legend, the reader is referred to the web version of this paper.)

binding may be a reasonable configuration because other monomer units could be extended through the methyl and hydroxymethyl groups.

The energy minimizations predicted three moderate strength H-bonds, where silanols acted as proton donors, and one weak H-bond, where a silanol acted as a proton acceptor (Fig. 4a). The H-bond distances between silanols of OHS and DET hydroxyls (≡SiO—H···OH—C—) were 1.92, 1.96, and 2.05 Å, and the distance of the weak H-bond between a silanol and a hydrogen of the DET ring (≡SiHO···H—C—) was 2.49 Å (Table 2). Interactions of the DET with (−1) negatively charged OHS ($^{-}$OHS) reduced the H-bond distances to 1.48, 1.88, and 1.95 Å mainly due to the H-bond between ≡Si—O^{-} and hydroxyl of DET (Fig. 4d). However, the weak H-bond increased to 3.10 Å due to the interaction with $^{-}$OHS.

DET has a stronger binding energy with a charged surface of OHS ($^{-}$OHS) than a neutral surface of OHS (Table 2). The binding energies were −9 kJ/mol for DET/OHS and −53 kJ/mol for DET/$^{-}$OHS. The deformation energy was higher in the interactions with $^{-}$OHS than OHS.

3.2.2. PHO with OHS

Energy minimization of PHO/OHS started based on the energy-minimized structure of DET/OHS. The energy-minimization predicted that two hydroxyls and two phosphate oxygens of PHO formed four H-bonds with silanols groups of OHS (Fig. 4b). The four silanols acted as proton donors in the H-bonds. The H-bond distances between the ≡Si—OH and the phosphate group (≡SiO—H···O—PO_4H—) were 1.64 and 1.68 Å, which were shorter than the H-bond distances observed in LYS/OHS and DET/OHS dimers (Table 2). The distances between DET hydroxyls and OHS silanols groups were 1.82 and 1.85 Å.

In contrast to the DET interactions, interactions of PHO with the negatively charged OHS increased the intermolecular distance of the dimer because of interactions between a phosphate oxygen and ≡Si—O^{-} (Fig. 4e). The

Table 2
H-bond distance, BSSE, enthalpy correction, deformation energy, and BSSE corrected binding energy of monomeric units with neutral OHS and negatively charged OHS calculated with B3LYP/6-311++G(d,p)//HF/3-21G(d,p)

	DET		PHO		LYS	
	OHS	$^{-}$OHS[b]	OHS	$^{-}$OHS[b]	OHS	$^{-}$OHS[b]
Distance[a] [Å]	1.92	1.48	1.64	1.65	1.72	1.77
	1.96	1.88	1.68		1.81	1.77
	2.05	1.95	1.82	1.80	1.86	1.84
	2.49[†]	3.10[†]	1.85	1.96	2.98[†]	1.72
ΔH Correction[c] (kJ/mol)	15.1	9.8	16.8	13.1	14.4	13.8
BSSE (kJ/mol)	17.6	19.4	23.1	19.4	16.7	21.9
E_{DEF}[d] (kJ/mol)	16.4	47.9	23.2	25.3	29.2	83.0
ΔH_{bind}[e] (kJ/mol)	−9	−53	−129	+158	−86	−278

[a] H-bond distances between silanol groups of OHS and functional groups of monomeric units (see Fig. 4. Note that the distances[†] are weak H-bonds between alkyl H and silanol O).
[b] $^{-}$OHS, OHS taking (−1) charge due to deprotonation of one silanols group on OHS.
[c] Zero-point energy and thermal energy correction for enthalpy calculations at 1 atm and 298 K.
[d] Deformation energy of monomers.
[e] BSSE corrected binding energy.

H-bond distances of the phosphate were 1.65 Å with ≡Si—OH, and the corresponding distance was 4.91 Å with ≡Si—O^{-}. The H-bond distances of OH groups with silanols were 1.80 and 1.96 Å.

The binding energy of PHO with OHS was stronger than the other monomers, but the strong repulsion was predicted between PHO with $^{-}$OHS (Table 2). The BSSE corrected binding energies were −129 kJ/mol for PHO/OHS and +158 kJ/mol for PHO/$^{-}$OHS. A previous ab initio study reported strong H-bonds between phosphates and neutral silanols with ca. −60 kJ/mol per H-bond (Murashov and Leszczynski, 1999). Our results are consistent for the neutral model, but the negative surface charge of quartz under most pH conditions should be included in the model calculations in order to be realistic. This issue is discussed in more detail below.

3.2.3. LYS with OHS

Energy minimization of LYS/OHS predicted three moderate H-bonds and one weak H-bond with silanols (Fig. 4c). Silanols acted as H-acceptors in the two moderate H-bonds via an amine group in a side chain (NH_3^+) (≡SiHO···H—NH_2—) and in one weak H-bond through a H of LYS backbone (≡SiHO···H—C—). The H-bond distances between the amine group and silanols were 1.81 and 1.86 Å, and the weak H-bond distance was 2.98 Å (Table 2). The silanol in the moderate H-bond through C=O in the amide group (CONH) acted as a proton donor (≡SiO—H···O=C—). For the peptide H-bonds, two different starting structures were tested:

(1) N—H group of an amide forms a H-bond to a silanol of OHS, and
(2) C=O group of an amide forms a H-bond to a silanol of OHS.

Both initial structures were energy minimized by favoring a H-bond formation of the carbonyl group to a silanol with a distance of 1.72 Å due to the stronger H-bond of C=O than the N—H with ≡Si—OH (Åquino et al., 2003). When a silanol H was taken off to form $^{-}$OHS, the amide group formed two H-bonds with distances of 1.77 Å (≡SiO—H···O=C—) and 1.72 Å (≡Si—O^{-}···HN—) (Fig. 4f). The other H-bond distances were 1.77 and 1.84 Å.

The interaction of positively charged LYS with negatively charged $^{-}$OHS was stronger than interaction with neutral OHS as well as any other dimer interactions (Table 2). The BSSE corrected binding energies were −86 kJ/mol for LYS/OHS and −278 kJ/mol for the LYS/$^{-}$OHS. The deformation energy was higher in the interactions with $^{-}$OHS than OHS similar to the DET interactions.

3.3. Analysis of binding energies with OHS

3.3.1. Silanol IR frequencies and the intensities

As mentioned in the Introduction, red-shifting (i.e., decreasing frequency) and increasing intensity of O—H stretching vibrations are indicators of H-bond strength. Thus, to analyze the nature of the dimer interaction energy, we examined the changes in vibrational frequency and intensity of the OH groups involved in binding the dimers.

The silanol O—H stretching vibrational frequencies and the IR intensities changed dramatically according to different H-bonds of dimers, whereas the OH bond distance variation did not (0.94–0.97 Å) (Table 3). The dimer with a higher binding energy had a lower OH vibrational frequencies. The binding energies and the lowest frequencies of the PHO/OHS, LYS/OHS, and DET/OHS were −129, −86, and −9 kJ/mol, and 3640, 3912, and 4094 cm^{-1}, respectively. The OH frequency of isolated OHS was 4286 cm^{-1}. The IR intensities of PHO/OHS and LYS/OHS increased up to almost 1400×10^2 cm^{-2}/mol/L from 299×10^2 cm^{-2}/mol/L (intensity of a non-H-bonded silanol), whereas the intensities of DET/OHS increased up to 900×10^2 cm^{-2}/mol/L.

Table 3
Calculated vibrational frequencies[a] of stretching silanol OH and stabilizing energies[b] caused by interactions between occupied and empty anti-bonding orbitals in the dimer H-bonds

Hydrogen bonds	Silanol OH bond distance (Å)	Silanol OH frequency[a] (cm^{-1})	Orbital interactions	Electron occupancy[d]	Stabilizing energy[b] (kJ/mol)
DET/OHS					
≡SiO—H···OH—C—	0.96	4080 (176)	$O_{LP(COH)} \rightarrow \sigma^*H—O_{Si}$	0.018	30.7
≡SiO—H···OH—C—	0.95	4088 (197)	$O_{LP(COH)} \rightarrow \sigma^*H—O_{Si}$	0.014	21.0
≡SiO—H···OH—C—	0.94	4094 (898)	$O_{LP(COH)} \rightarrow \sigma^*H—O_{Si}$	0.012	17.2
≡SiHO[e]···H—C—	0.94	4271[c] (168)			
LYS/OHS					
≡SiO—H···O=C—	0.95	3912 (1389)	$O_{LP(O=C)} \rightarrow \sigma^*H—O_{Si}$	0.038	65.5
≡SiHO···H—NH_2–	0.94	4224[c] (278)	$O_{LP(OHS)} \rightarrow \sigma^*H—N$	0.034	55.9
≡SiHO···H—NH_2–	0.94	4225[c] (138)	$O_{LP(OHS)} \rightarrow \sigma^*H—N$	0.032	44.6
≡SiHO[e]···H—C—	0.94	4278[c] (210)			
PHO/OHS					
≡SiO—H···O—PO_4H—	0.97	3640 (1009)	$O_{LP(O—P)} \rightarrow \sigma^*H—O_{Si}$	0.045	104.7
≡SiO—H···O—PO_4H—	0.96	3729 (1321)	$O_{LP(O—P)} \rightarrow \sigma^*H—O_{Si}$	0.036	80.9
≡SiO—H···OH—C—	0.95	3990 (394)	$O_{LP(COH)} \rightarrow \sigma^*H—O_{Si}$	0.027	47.4
≡SiO—H···OH—C—	0.95	4026 (1022)	$O_{LP(COH)} \rightarrow \sigma^*H—O_{Si}$	0.023	43.7

O_{LP}, lone pair electrons of occupied oxygen orbitals; σ^*, empty anti-bonding orbital of OH or NH bond.
[a] Vibrational frequencies (HF/3-21G(d,p)//HF/3-21G(d,p)) were not scaled. The values in parentheses are IR intensity (10^2 cm^{-2}/mol/L). Note that the OH frequency of bare OHS was 4286 cm^{-1} with the IR intensity of 299×10^2 cm^{-2}/mol/L at 0.93 Å bond distance.
[b] Estimated with 2nd-order perturbation theory in NBO analysis (Reed et al., 1988) in a B3LYP/6-311++G(d,p) level.
[c] OH frequency of a silanol, which is a hydrogen acceptor.
[d] Number of electrons occupied in anti-bonding orbitals after the negative hyperconjugation.
[e] Weak hydrogen bond.

Note that the frequencies reported in the Table 3 were not scaled to correct the HF level overestimation.

3.3.2. Natural bond orbital (NBO) analysis

Another component of the dimer interaction energy is the electron transfer between orbitals on each subunit (i.e., electrons moving from orbitals on a monomer to OHS or vice versa). This electron transfer is related to the H-bonding energy, so this analysis complements the results discussed above.

Analysis of the interactions between the NBO orbitals of dimers found that the major interactions in the dimers were between lone pair electrons of H acceptors in the H-bonds and anti-bonding orbitals of O—H in the silanols or N—H in the amine (i.e., $O_{LP} \rightarrow \sigma^*_{H—O}$or $O_{LP} \rightarrow \sigma^*_{H—N}$) (Table 3). Stabilization energies of the weak H-bond between the alkyl H and the silanol O were negligible compared to the energies of other H-bonds.

Dimers with stronger binding energy had more electrons transferred from the occupied orbitals to empty orbitals and thus greater stabilization energy. The interactions of PHO phosphate oxygen orbitals with silanol OH anti-bonding orbitals ($O_{LP(O—P)} \rightarrow \sigma^*_{H—OSi}$) transferred 0.045 electrons with 104.7 kJ/mol stabilizing energy. The interactions of LYS carbonyl oxygen orbitals ($O_{LP(O=C)} \rightarrow \sigma^*_{H—OSi}$) and the ones of DET hydroxyl oxygen orbitals ($O_{LP(COH)} \rightarrow \sigma^*_{H—OSi}$) transferred 0.38 electrons with 65.5 kJ/mol and 0.018 electrons with 30.7 kJ/mol, respectively.

3.4. Solvent effects on binding strength

The type of solvent (i.e., high or low dielectric constant) affected the absolute strength of binding energy

Table 4
Interaction energies and solvation energies of dimers calculated with the conductor-like polarizable continuum (C-PCM) model (Klamt and Schuurmann, 1993) and B3LYP/6-311++G(d,p) based on the energy-minimized structures in a gas phase

Solvent	DET/OHS		PHO/OHS		LYS/OHS	
	ΔE[a]	$\Delta\Delta G_{sol}$[b]	ΔE[a]	$\Delta\Delta G_{sol}$[b]	ΔE[a]	$\Delta\Delta G_{sol}$[b]
Water ($\varepsilon = 78.39$)	−64.6	84.8	−202.0	148.2	−154.2	150.1
Ethanol ($\varepsilon = 24.55$)	−66.3	73.5	−205.9	161.2	−156.7	133.0
Heptane ($\varepsilon = 1.92$)	−60.2	35.6	−195.5	84.2	−149.2	65.9
Gas ($\varepsilon = 1.00$)	−53.9		−191.7		−146.0	

Unit, kJ/mol. ε is dielectric constant at 20 °C (Laurence et al., 1994). Note that dielectric constant of perfluorodecalin (PFD) is 1.86 (Abboud and Notario, 1999 and references therein).
[a] E, internal energy in a continuum cavity without BSSE and enthalpy correction ($\Delta E = -(E_{MON} + E_{OHS} - E_{MON/OHS})$).
[b] ΔG_{sol}, electrostatic + non-electrostatic solvation energy ($\Delta\Delta G_{sol} = -(\Delta G_{sol,MON} + \Delta G_{sol,OHS} - \Delta G_{sol,MON/OHS})$).

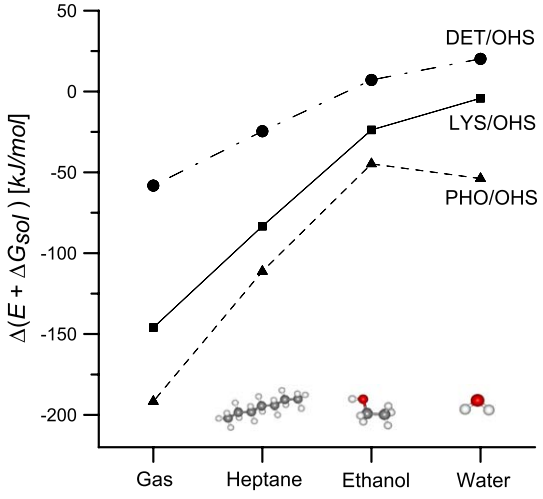

Fig. 5. Interaction energy of DET/OHS (circle), PHO/OHS (triangle), and LYS/OHS (square) in different solvents calculated using a continuum solvent model.

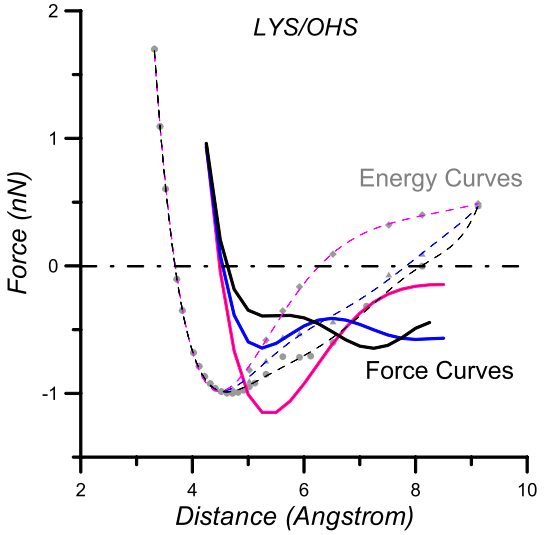

Fig. 6. LYS/OHS potential energy curves (dashed lines) and their force curves (solid lines) derived from the energy curves as a function of dimer distance. Note that the energy curves and, in particular, the force curves strongly depended on the number of fixed LYS carbon atoms: diamond and red lines with six carbon atoms fixed (the maximum attractive force: −1.16 nN); triangle and blue lines with four carbon atoms fixed (the maximum attractive force: −0.64 nN); circle and black lines with three carbon atoms fixed (the maximum attractive force: −0.39 nN). (For interpretation of the references to color in this figure legend, the reader is referred to the web version of this paper.)

but did not affect the calculated relative strength among the dimers (Table 4). The binding strength increased in solvents with a lower dielectric constant (Fig. 5). For example, the interaction energies ($\Delta(E+\Delta G_{sol})$), which can indicate the binding strength, became more negative from water to ethanol to heptane. This trend agrees well with the experimental observation that solvents with a low dielectric constant increased the adhesion force between polar surfaces such as hydroxyl functional groups (Papastavrou and Akari, 2000). In particular, the energies in a heptane, which has a dielectric constant close to PFD one ($\varepsilon = 1.86$) (Abboud and Notario, 1999), were much stronger than those in H_2O by approximately one order of magnitude. The stronger binding strength in heptane than in H_2O is consistent with the pull-off force enhancement from H_2O to PFD media observed in this study. The relative binding strengths of each dimer in a calculated in the gas phase were qualitatively same as the relative binding strength in heptane, ethanol, and water solvents.

3.5. Force curves from potential energy curves

The measured force data may be compared to force curves derived from the calculated dimer potential energies through Eq. (3). However, the force curves of the LYS/OHS dimer showed limitations in the use of the derived forces for comparison with experimental data. As mentioned in the computational details above, geometry constraints are necessary in predicting potential energy curves, but the derived forces strongly depended on the number of fixed atoms in the LYS/OHS (Fig. 6). Thus, quantitative comparison of the model force curves to experiment (in particular, curves of the more flexible LYS compared to DET and PHO structures) is prevented in this case.

4. Discussion

4.1. H-bond strength and relative binding strength

The calculated binding energies of the polymeric monomers with negatively charged OHS ($^{-}$OHS) can be understood as electrostatic interactions (Table 2): the positively charged LYS would have attractive interactions with $^{-}$OHS (−278 kJ/mol), negatively charged PHO would have repulsive interactions with $^{-}$OHS (+158 kJ/mol), and the neutral DET would be between the two interactions (−53 kJ/mol).

The binding energies with neutral OHS are not as straightforward as the $^{-}$OHS case, however. The negatively charged PHO showed stronger interactions with neutral OHS (−129 kJ/mol) than the positively charged LYS (−86 kJ/mol). The neutral DET had the weakest interaction energy with the neutral OHS (−9 kJ/mol). Because the neutral OHS is an important model as well as $^{-}$OHS representing silica surfaces in low to circum-neutral pH solution, detailed analysis on interactions of polymer units with neutral OHS is necessary.

In general, the shorter the H-bond distance, the more red-shifted the silanol OH stretching vibration frequency, the greater the increase in OH stretch IR intensity, and the more electron transfer from O orbitals to anti-bonding orbitals of silanols ($O_{LP} \rightarrow \sigma^{*}_{H-O}$), the stronger the H-bonding. All four analyses here showed that PHO/OHS has stronger H-bonding than LYS/OHS and DET/

OHS. The H-bond distance between a silanol and the phosphate of PHO (1.64 Å) was shorter than the distances of carbonyl of LYS (1.72 Å) and hydroxyls of DET (1.92 Å) (Table 2). The relative vibrational frequency shifts of H-bonded silanol OH from the non-H-bond silanol OH frequency (4286 cm^{-1}) were 15% in PHO/OHS, 9% in LYS/OHS, and 5% in DET/OHS (Table 3). In addition, the stabilization energy in PHO/OHS due to the negative hyperconjugation ($O_{LP} \rightarrow \sigma^*_{H-O}$) was much higher than the energies in LYS/OHS and DET/OHS (Table 3). The analyses of H-bond distances, IR vibrational frequencies and intensities of silanols, and stabilization energy from orbital interactions indicate that the different H-bond strength of dimers determined the relative binding energy with the neutral OHS.

4.2. Solvent effects on the binding strength

The significant enhancement of pull-off forces in PFD can be attributed to the low dielectric constant enhancing H-bonding effects between the monomers and the OHS and $^{-}$OHS in the absence of H-bonding to the solvent. Although several parameters (e.g., solvent radius and density) in addition to a dielectric constant are used in the CPCM calculation, the strong correlation between the interaction energies ($\Delta(E+\Delta G_{sol})$), which represent the binding strengths of dimers, and dielectric constants of solvents indicates that a low dielectric constant solvent enhanced the interaction strength (Fig. 5).

The dependence of binding strengths on dielectric constants can be explained with solvation-energy difference between a dimer and the separate monomers ($\Delta\Delta G_{sol}$) because the $\Delta\Delta G_{sol}$ determined the relative change of $\Delta(E+\Delta G_{sol})$ with the change of dielectric constants. The $\Delta\Delta G_{sol}$ were all positive and changed significantly depending on solvents that have different dielectric constants, whereas the internal energies (ΔE) were not much different from solvent to solvent (Table 4). Note that the more polar solvent, water, had the more positive $\Delta\Delta G_{sol}$. The more positive $\Delta\Delta G_{sol}$ means that the binding dimer structure is the less favorable compared to the isolated monomers. Consequently, dimers in the more polar solvents produce a lower binding energy.

The more positive $\Delta\Delta G_{sol}$ in the more polar solvent is attributed to the decrease of attractive parts and the increase of non-attractive parts of isolated monomers to polar solvents in the dimer interactions, because the interactions between the two monomers limit the attractive parts of each monomer available to polar solvents (Åquino et al., 2002). For example, intermolecular H-bonds between two monomers can decrease the number of H-bonds of monomers available to a polar solvent.

The different order of the measured binding strengths of polymers in water and PFD media is attributed to the different surface charges of polymers and silica in the solvents. In water, the polymers and silica surfaces are expected to take on their own charges from their proton dissociation constants and isoelectric points. However, in the PFD solvent, the polymers and silica probably would not take on any charges because PFD ($C_{10}F_{18}$) is not a protic acid or base. As shown in the binding energies of PHO with neutral OHS and negatively charged $^{-}$OHS (Table 2), the different charge conditions resulted in similar pull-off forces of DET and PHO in water and similar to the forces of LYS and PHO in PFD (Fig. 3).

4.3. Binding energies and normalized pull-off forces

The relative binding strengths of polymers determined from the normalized pull-off forces measured in water were in context of the calculated binding energies in a gas phase. The main reason for the use of gas-phase calculations is that the enthalpy was not clearly determined in the continuum solvent treating calculations such as PCM. In addition, as observed in the solvent effects above, the change of solvent from water to a gas phase qualitatively did not affect the relative binding strength.

The current dimer models overestimated the binding energies. Amorphous colloidal silica, which was used in the force measurements, is known to have lower hydroxyl density than a quartz crystal (Zhuravlev, 1987), and colloidal silica takes on smaller fractional charges per nm^2 (Cardenas, 2005). Because the model OHS was made based on a surface with apparent charges of zero and negative (−1) charge with approximately 25 $Å^2$ of OHS, the binding energies of dimers were overestimated. The overestimation of binding energy was corrected based on the silica surface hydroxyl density and the silica surface charge density.

4.3.1. Silica surface hydroxyl density

Previous studies on amorphous silica have shown that the OH density is 4.6–4.9 OH groups per nm^2 depending on deuterium or tritium exchange method (Zhuravlev, 1987; Zhuravlev, 2000). The model OHS structure used in this study has a similar skeleton as quartz (5 Å between silanols), so the OH density of the OHS model corresponds to 16 OH per nm^2, which is higher than the experimental values by approximately three times. To consider the low packing density of amorphous silica used in AFM experiments, the OH density correction should be included in the comparison of calculated binding energy with the measured AFM data. Therefore, the OH density correction was made by multiplying the BSSE corrected enthalpy for the binding energy by 5/16. This correction makes the number of polymeric units physically interacting silica surface one unit from four units per nanometer squares of the silica surface.

4.3.2. Silica surface charge density

Although silica surfaces can be negatively charged above pH 2, the surface charges do not increase dramatically up to pH 8. A recent XPS study on colloidal SiO_2 particles has shown that the surface charge density (σ) of the silica is between −0.019 and −0.067 C/m^2 at the pH 2–8 in

20 mM NaCl aqueous solution (Cardenas, 2005). The σ corresponds to approximately −0.1 to −0.4 equivalent charge per nm^2. In this sense, instead of $^-$OHS, the use of neutral OHS is closer to the real surface charge of silicas. However, consideration of a fractional surface-charge density of OHS is warranted to account for the electrostatic effects. For example, fractional negative charges on OHS would compensate for the overestimated PHO/OHS energy as electrostatic repulsion decreases the magnitude of the interaction energy.

Binding energies at the fractional surface charge density were estimated by interpolation with the binding energies of the two end-members at the neutral OHS and charged $^-$OHS. For example, the summation of 90% DET/OHS binding energy and 10% DET/$^-$OHS binding energy gives the binding energy at the surface charge of −0.1 equivalent charge/nm^2 (i.e., −0.016 C/m^2). The estimated binding energies are plotted in Fig. 7 as a function of the surface charge density. Solution pH conditions, where surface charge density of colloidal silica was determined in 20 mM NaCl aqueous solution (Cardenas, 2005), were also expressed in Fig. 7 to present the qualitative dependence of surface charge density on the solution pH. Quantitative matches between the pH condition and OHS charge density should be avoided in this case.

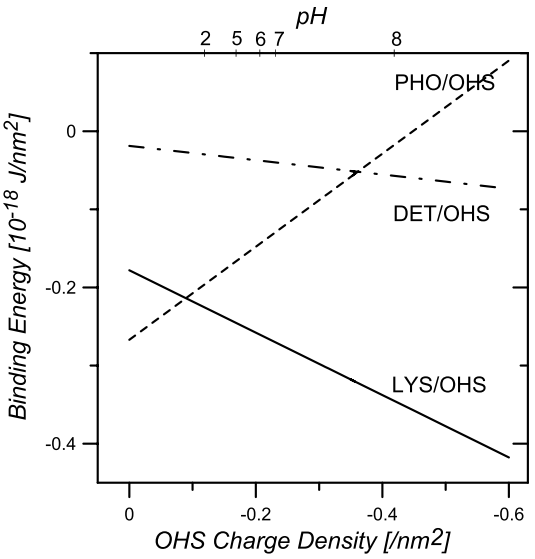

Fig. 7. Binding energy of dimers as a function of the OHS surface change density. Note that the pH axis based on the data of Cardenas (2005) is presented in order to show qualitative dependence of silica surface charge density on solution pH.

The fractional surface charges on OHS brought the relative binding strength of the model dimers in better agreement with the measured binding strength of polymers. For example, the binding energies of DET and PHO became similar in the −0.3 to −0.4 equivalent charges/nm^2 range, which approximates circum-neutral solution pH range, as in the measured pull-off forces of dextran and phosphorylated dextran (Table 5).

Although the relative strength of dimer binding energies is in good agreement with the measured pull-off forces, the LYS binding energy in the neutral pH range was still overestimated compared to the other dimers. The overestimation can be attributed to the high charge densities of modeled polymeric unit (e.g., +1 on the poly-L-lysine unit model) interacting with OHS. Just as silica surfaces, the homopolymers attached to the slide glasses would take smaller fractional charges rather than the (+1) LYS. For example, recent second harmonic generation (SHG) studies have estimated the interfacial charge densities of organic molecules on SAM interface as low as 0.0003 C/m^2 for carboxyl-terminated SAM to 0.02 C/m^2 for 15-mer oligonucleotide SAM at around pH 7 (Konek et al., 2004; Boman et al., 2005). Thus, correction for the surface charge density on the polymeric units would produce more realistic binding energies.

4.3.3. Implications

The AFM pull-off force measurements with electronic structure calculations have shown that phosphates can form relatively strong interactions with silica surfaces. Orthophosphates and phosphate groups in EPS are known to form covalent bonds to Fe-hydroxides (Persson et al., 1996; Omoike et al., 2004). Although the H-bonding interactions inferred here are significant, they are not comparable in strength to the strong bonding between phosphates and Fe-hydroxides. On the other hand, the adhesion strength between phosphates and silica surface has been underestimated because of the assumption that negatively charged phosphates would not adsorb significantly to negatively charged silica surfaces. In this study, however, the PHO representing phosphate containing polymers (e.g., denatured nucleic acids or phospholipids) had stronger

Table 5
Calculated binding energies[e] per unit area (10^{-18} J/nm^2) of OHS with surface OH density and surface charge density corrections

	OHS[a]	(−)OHS[b]	$\sigma^c = -0.3$ (/nm^2)	$\sigma^c = -0.4$ (/nm^2)	Exp[d]
DET	−0.019	−0.110	−0.046	−0.055	−0.026 (±0.005)
PHO	−0.267	+0.329	−0.088	−0.029	−0.022 (±0.004)
LYS	−0.178	−0.577	−0.298	−0.338	−0.061 (±0.007)

[a] OHS, surface charge density is zero.
[b] (−)OHS, OHS taking (−1) charge due to deprotonation of one silanols group on OHS. The surface charge density is −1 (/nm^2).
[c] σ, surface charge density of OHS.
[d] Normalized energies (10^{-18} J/nm^2) derived from the measured forces of dextran, phosphorylated dextran, and poly-L-lysine in H_2O (see Table 1).
[e] BSSE corrected enthalpy (see text).

binding energy than the LYS (analogue to positively charged proteins) at the low surface charge from zero to approximately −0.1 equivalent charge/nm^2 (Fig. 7). The −0.1 equivalent charge/nm^2 matches the surface charge density of colloidal silica at approximately pH 2 in 20 mM NaCl and pH 4 in 100 mM KCl (Cardenas, 2005). In addition, PHO binding energy was greater than DET (analogue to neutral polysaccharides) binding energy at up to −0.35/nm^2 of the surface charge density. Because the binding strength of PHO/OHS is more sensitive than DET/OHS to the change of a solvent from a gas phase to a water solvent (Fig. 5), the intercept between the binding energy lines of PHO/OHS and DET/OHS would shift to the lower pH when the water solvent is considered. Thus, the pH condition corresponding to −0.35/nm^2 would be in the range of 6–7 based on the Cardenas data in 20 mM NaCl (2005). Granted the uncertainty and difficulty in the direct quantitative conversion of solution pH from the simulated OHS surface charge in a gas phase, this study implies that phosphate-containing polymers have relatively strong adhesion with silica surfaces at low pH compared to polysaccharides and proteins.

One complication that must be considered in phosphate/silica interactions is the explicit H_2O molecules in the hydration of phosphates and silica surfaces. H_2O molecules strongly H-bond to anions and may hinder phosphate adsorption to silica surfaces. However, a previous study has shown that the H-bonds of a phosphate with two silanols are stronger than the doubly hydrated phosphate by approximately 8 kJ/mol per H-bond (Murashov and Leszczynski, 1999). Furthermore, in this study, we attempted to simulate the detachment energy corresponding to the pull-off forces, of polymers from the silica surface after attachment to the surface rather than the initial adhesion step. This study implies that once the phosphate-containing polymers bind to the silica surface, higher energy is needed to separate the polymers from silica surfaces due to the strong H-bonds compared to other polymers.

5. Conclusions

The roles of three components of complex EPS interactions with silica surfaces were investigated with AFM and electronic structure calculations. This study provides fundamentals on the nature of interactions such as the dominant forces (H-bonds and electrostatic interactions) and the binding strength between major components of EPS with silica. The current study suggests that the phosphate-containing polymers, such as DNA and phospholipids, would be major components in EPS responsible for the adhesion strength with silica surfaces at low pH, possibly up to neutral pH.

Previous IR and Raman spectroscopic studies have shown that phosphoryl groups of a DNA backbones are the main functional groups in the DNA sticking to silica (Mao et al., 1994; Mercier and Savoie, 1997). This is consistent with our results that phosphates form stronger H-bonds with neutral silanols (≡SiOH) than other functional groups of polymers:

(1) the stronger binding energy of PHO with neutral OHS,
(2) the greater red-shifting of silanol vibrational frequencies in PHO/OHS (ca. 15% relative shift), and
(3) the greater electron charge transfer from oxygen lone pair electrons to silanol hydroxyl anti-bonding orbitals in PHO/OHS.

In addition, our electronic structure calculations showed that H-bonds become dominant forces between phosphates and neutral silanols, whereas electrostatic interactions are dominant between phosphates and deprotonated silanol (≡SiO$^-$) that is a general surface group of silica in a high pH solution. The dominant H-bonds in a low pH solution explain the experimental observation that more DNA adsorb to silica and sand at lower pH (Lorenz and Wackernagel, 1987; Romanowski et al., 1991; Melzak et al., 1996).

A methodology was developed to analyze measured AFM forces with cluster-type electronic structure calculations. Pull-off forces (minima in retraction force curves) of homopolymers measured with a silica colloid were normalized with the effective silica surface area contacting the polymer surfaces. The normalized pull-off forces were compared to binding energies (enthalpy required to separate dimers into two isolated monomers) calculated from the full energy-minimizations of dimer structures representing the interactions between homopolymers and a silica colloid. The overestimated binding energies due to the cluster approximation can be partly corrected by charge density and silanol density of silica surface.

Acknowledgments

This research was supported by NSF-Collaborative Research Activities in Environmental Molecular Sciences (CRAEMS) (Grant CHE-0089156) and ACS-Petroleum Research Fund (PRF) (Grant 41132-AC2). Computation was supported in part by the Materials Simulation Center, a Penn State MRSEC and MRI facility and the Center for Environmental Kinetics Analysis (CEKA—an NSF/DOE Environmental Molecular Sciences Institute). The authors thank three anonymous reviewers for valuable comments in greatly improving the content and presentation of the manuscript. K.K. acknowledges support from the Penn State Biogeochemical Research Initiative for Education (BRIE) sponsored by NSF (IGERT) (Grant DGE-9972759) and Dr. Li-Chong Xu and Charles Winslow for helpful discussion on AFM experiments and Yongcheol Park for help of Matlab programming.

Associate editor: Jeremy B. Fein

References

Abboud, J.L.M., Notario, R. 1999. Critical compilation of scales of solvent parameters. Part I. Pure, non-hydrogen bond donor solvents—Technical report. *Pure Appl. Chem.* **71**, 645–718.

Åquino, A.J.A., Tunega, D., Haberhauer, G., Gerzabek, M.H., Lischka, H., 2002. Solvent effects on hydrogen bonds—a theoretical study. *J. Phys. Chem. A* **106**, 1862–1871.

Åquino, A.J.A., Tunega, D., Haberhauer, G., Gerzabek, M.H., Lischka, H., 2003. Adsorption of organic substances on broken clay surfaces: a quantum chemical study. *J. Comput. Chem.* **24**, 1853–1863.

Ashby, P.D., Chen, L., Lieber, C.M., 2000. Probing intermolecular forces and potentials with magnetic feedback chemical force microscopy. *J. Am. Chem. Soc.* **122**, 9467–9472.

Bach, R.D., Dmitrenko, O., Glukhovtsev, M.N., 2001. A theoretical study of the effect of a tetraalkylammonium counterion on the hydrogen bond strength in Z-hydrogen maleate. *J. Am. Chem. Soc.* **123**, 7134–7145.

Barone, V., Cossi, M., Tomasi, J., 1997. A new definition of cavities for the computation of solvation free energies by the polarizable continuum model. *J. Chem. Phys.* **107**, 3210–3221.

Becke, A.D., 1993. Density-functional thermochemistry. 3. The role of exact exchange. *J. Chem. Phys.* **98**, 5648–5652.

Becker, K., 1996. Exopolysaccharide production and attachment strength of bacteria and diatoms on substrates with different surface tensions. *Microb. Ecol.* **32**, 23–33.

Boman, F.C., Musorrafiti, M.J., Gibbs, J.M., Stepp, B.R., Salazar, A.M., Nguyen, S.B.T., Geiger, F.M., 2005. DNA single strands tethered to fused quartz/water interfaces studied by second harmonic generation. *J. Am. Chem. Soc.* **127**, 15368–15369.

Boys, S.F., Bernardi, F., 2002. The calculation of small molecular interactions by the differences of separate total energies. Some procedures with reduced errors (Reprinted from Molecular Physics, vol. 19, p. 553–566, 1970). *Mol. Phys.* **100**, 65–73.

Cappella, B., Dietler, G., 1999. Force–distance curves by atomic force microscopy. *Surf. Sci. Rep.* **34**, 1–104.

Cardenas, J.F., 2005. Surface charge of silica determined using X-ray photoelectron spectroscopy. *Colloid Surf. A-Physicochem. Eng. Asp.* **252**, 213–219.

Chalasiński, G., Szczęśniak, M.M., 2000. State of the art and challenges of the *ab initio* theory of intermolecular interactions. *Chem. Rev.* **100**, 4227–4252.

Chan, C.S., De Stasio, G., Welch, S.A., Girasole, M., Frazer, B.H., Nesterova, M.V., Fakra, S., Banfield, J.F., 2004. Microbial polysaccharides template assembly of nanocrystal fibers. *Science* **303**, 1656–1658.

Chilkoti, A., Boland, T., Ratner, B.D., Stayton, P.S., 1995. The relationship between ligand-binding thermodynamics and protein–ligand interaction forces measured by atomic force microscopy. *Biophys. J.* **69**, 2125–2130.

Cossi, M., Rega, N., Scalmani, G., Barone, V., 2003. Energies, structures, and electronic properties of molecules in solution with the C-PCM solvation model. *J. Comput. Chem.* **24**, 669–681.

Costerton, J.W., Marrie, T.J., Cheng, K.-J., 1985. Phenomena of bacterial adhesion. In: Savage, D.C., Fletcher, M. (Eds.), *Bacterial Adhesion*. Plenum Press, New York, pp. 3–43.

Cramer, C.J., Truhlar, D.G., 1999. Implicit solvation models: Equilibria, structure, spectra, and dynamics. *Chem. Rev.* **99**, 2161–2200.

Dade, W.B., Davis, J.D., Nichols, P.D., Nowell, A.R.M., Thistle, D., Trexler, M.B., White, D.C., 1990. Effects of bacterial exopolymer adhesion on the entrainment of sand. *Geomicrobiol. J.* **8**, 1–16.

Duval, Y., Mielczarski, J.A., Pokrovsky, O.S., Mielczarski, E., Ehrhardt, J.J., 2002. Evidence of the existence of three types of species at the quartz-aqueous solution interface at pH 0–10: XPS surface group quantification and surface complexation modeling. *J. Phys. Chem. B* **106**, 2937–2945.

Evans, E., 2001. Probing the relation between force—Lifetime—and chemistry in single molecular bonds. *Annu. Rev. Biochem.* **30**, 105–128.

Evans, E., Ritchie, K., 1997. Dynamic strength of molecular adhesion bonds. *Biophys. J.* **72**, 1541–1555.

Feldmann, K., Tervoort, T., Smith, P., Spencer, N.D., 1998. Toward a force spectroscopy of polymer surfaces. *Langmuir* **14**, 372–378.

Fletcher, M., 1996. Bacterial attachment in aquatic environments: a diversity of surfaces and adhesion strategies. In: Fletcher, M. (Ed.), *Bacterial Adhesion: Molecular and Ecological Diversity*. John Wiley, New York, pp. 1–24.

Florin, E.L., Moy, V.T., Gaub, H.E., 1994. Adhesion forces between individual ligand–receptor pairs. *Science* **264**, 415–417.

Frey, B.L., Corn, R.M., 1996. Covalent attachment and derivatization of poly(L-lysine) monolayers on gold surfaces as characterized by polarization-modulation FT-IR spectroscopy. *Anal. Chem.* **68**, 3187–3193.

Frisch, M.J., Delbene, J.E., Binkley, J.S., Schaefer, H.F., 1986. Extensive theoretical-studies of the hydrogen-bonded complexes $(H_2O)_2$, $(H_2O)_2H^+$, $(HF)_2$, $(HF)_2H^+$, F_2H^-, and $(NH_3)_2$. *J. Chem. Phys.* **84**, 2279–2289.

Frisch, M.J., Trucks, G.W., Schlegel, H.B., Scuseria, G.E., Robb, M.A., Cheeseman, J.R., Montgomery Jr., J.A., Vreven, T., Kudin, K.N., Burant, J.C., Millam, J.M., Iyengar, S.S., Tomasi, J., Barone, V., Mennucci, B., Cossi, M., Scalmani, G., Rega, N., Petersson, G.A., Nakatsuji, H., Hada, M., Ehara, M., Toyota, K., Fukuda, R., Hasegawa, J., Ishida, M., Nakajima, T., Honda, Y., Kitao, O., Nakai, H., Klene, M., Li, X., Knox, J.E., Hratchian, H.P., Cross, J.B., Adamo, C., Jaramillo, J., Gomperts, R., Stratmann, R.E., Yazyev, O., Austin, A.J., Cammi, R., Pomelli, C., Ochterski, J.W., Ayala, P.Y., Morokuma, K., Voth, G.A., Salvador, P., Dannenberg, J.J., Zakrzewski, V.G., Dapprich, S., Daniels, A.D., Strain, M.C., Farkas, O., Malick, D.K., Rabuck, A.D., Raghavachari K., Foresman, J.B., Ortiz, J.V., Cui, Q., Baboul, A.G., Clifford, S., Cioslowski, J., Stefanov, B.B., Liu, G., Liashenko, A., Piskorz, P., Komaromi, I., Martin, R.L., Fox, D.J., Keith, T., Al-Laham, M.A., Peng, C.Y., Nanayakkara, A., Challacombe, M., Gill, P.M.W., Johnson, B., Chen, W., Wong, M.W., Gonzalez, C., Pople, J.A. 2003. Gaussian 03 (Revision B.5). Gaussian, Inc., Pittsburgh, PA.

Gordon, M.S., Binkley, J.S., Pople, J.A., Pietro, W.J., Hehre, W.J., 1982. Self-consistent molecular-orbital method. 22. Small split-valence basis sets for second-row elements. *J. Am. Chem. Soc.* **104**, 2797–2803.

Grubmüller, H., Heymann, B., Tavan, P., 1996. Ligand binding: Molecular mechanics calculation of the streptavidin biotin rupture force. *Science* **271**, 997–999.

Harrison, J.A., Stuart, S.J., Brenner, D.W., 1999. Atomic-scale simulation of tribological and related phenomena. In: Bhushan, B. (Ed.), *The Handbook of Micro/Nanotribiology*. CRC Press, Boca Raton, FL.

Hehre, W.J., Ditchfield, R., Pople, J.A., 1972. Self-consistent molecular orbital methods. XII. Further extension of Gaussian-type basis sets for use in molecular orbital studies of organic molecules. *J. Chem. Phys.* **56**, 2257–2261.

Hobza, P., Sponer, J., 1999. Structure, energetics, and dynamics of the nucleic acid base pairs: Nonempirical ab initio calculations. *Chem. Rev.* **99**, 3247–3276.

Hoh, J.H., Cleveland, J.P., Prater, C.B., Revel, J.P., Hansma, P.K., 1992. Quantized adhesion detected with the atomic force microscope. *J. Am. Chem. Soc.* **114**, 4917–4918.

Israelachvili, J.N., 1991. *Intermolecular and Surface Forces*. Academic Press, London.

Izrailev, S., Stepaniants, S., Balsera, M., Oono, Y., Schulten, K., 1997. Molecular dynamics study of unbinding of the avidin–biotin complex. *Biophys. J.* **72**, 1568–1581.

Jeffrey, G.A., 1997. *An Introduction to Hydrogen Bonding*. Oxford University Press, New York.

Johnson, K.L., Kendall, K., Roberts, A.D., 1971. Surface energy and the contact of elastic solids. *Proc. R. Soc. London, A* **324**, 301–313.

Jucker, B.A., Harms, H., Hug, S.J., Zehnder, A.J.B., 1997. Adsorption of bacterial surface polysaccharides on mineral oxides is mediated by hydrogen bonds. *Colloid Surf. B-Biointerfaces* **9**, 331–343.

Kendall, T.A., Hochella, M.F., 2003. Measurement and interpretation of molecular-level forces of interaction between the siderophore azotobactin and mineral surfaces. *Geochim. Cosmochim. Acta* **67**, 3537–3546.

Kendall, T.A., Hochella, M.F., Becker, U., 2005. Computational modeling of azotobactin-goethite/diaspore interactions: applications to molecular force measurements and siderophore-mineral reactivity. *Chem. Geol.* **216**, 17–35.

Klamt, A., Schuurmann, G., 1993. COSMO—a new approach to dielectric screening in solvents with explicit expressions for the screening energy and its gradient. *J. Chem. Soc., Perkin Trans.* **2**, 799–805.

Konek, C.T., Musorrafiti, M.J., Al-Abadleh, H.A., Bertin, P.A., Nguyen, S.T., Geiger, F.M., 2004. Interfacial acidities, charge densities, potentials, and energies of carboxylic acid-functionalized silica/water interfaces determined by second harmonic generation. *J. Am. Chem. Soc.* **126**, 11754–11755.

Konrad, M.W., Bolonick, J.I., 1996. Molecular dynamics simulation of DNA stretching is consistent with the tension observed for extension and strand separation and predicts a novel ladder structure. *J. Am. Chem. Soc.* **118**, 10989–10994.

Kreller, D.I., Gibson, G., Novak, W., Van Loon, G.W., Horton, J.H., 2003. Competitive adsorption of phosphate and carboxylate with natural organic matter on hydrous iron oxides as investigated by chemical force microscopy. *Colloid Surf. A-Physicochem. Eng. Asp.* **212**, 249–264.

Laurence, C., Nicolet, P., Dalati, M.T., Abboud, J.L.M., Notario, R., 1994. The empirical-treatment of solvent solute interactions: 15 years of π^*. *J. Phys. Chem.* **98**, 5807–5816.

Lee, C.T., Yang, W.T., Parr, R.G., 1988. Development of the Colle-Salvetti correlation-energy formula into a functional of the electron-density. *Phys. Rev. B* **37**, 785–789.

Leng, Y.S., Jiang, S.Y., 2002. Dynamic simulations of adhesion and friction in chemical force microscopy. *J. Am. Chem. Soc.* **124**, 11764–11770.

Lii, J.H., Ma, B.Y., Allinger, N.L., 1999. Importance of selecting proper basis set in quantum mechanical studies of potential energy surfaces of carbohydrates. *J. Comput. Chem.* **20**, 1593–1603.

Loaëc, M., Olier, R., Guezennec, J., 1997. Uptake of lead, cadmium and zinc by a novel bacterial exopolysaccharide. *Water Res.* **31**, 1171–1179.

Lorenz, M.G., Wackernagel, W., 1987. Adsorption of DNA to sand and variable degradation rates of adsorbed DNA. *Appl. Environ. Microbiol.* **53**, 2948–2952.

Lower, S.K., Tadanier, C.J., Hochella, M.F., 2000. Measuring interfacial and adhesion forces between bacteria and mineral surfaces with biological force microscopy. *Geochim. Cosmochim. Acta* **64**, 3133–3139.

Lynch, B.J., Zhao, Y., Truhlar, D.G., 2003. Effectiveness of diffuse basis functions for calculating relative energies by density functional theory. *J. Phys. Chem. A* **107**, 1384–1388.

Mao, Y., Daniel, L.N., Whittaker, N., Saffiotti, U., 1994. DNA-binding to crystalline silica characterized by Fourier-Transform infrared-spectroscopy. *Environ. Health Perspect.* **102** (Suppl. 10), 165–171.

Marcolli, C., Calzaferri, G., 1999. Monosubstituted octasilasesquioxanes. *Appl. Organomet. Chem.* **13**, 213–226.

Marshall, P.A., Loeb, G.I., Cowan, M.M., Fletcher, M., 1989. Response of microbial adhesives and biofilm matrix polymers to chemical treatments as determined by interference reflection microscopy and light section microscopy. *Appl. Environ. Microbiol.* **55**, 2827–2831.

Melzak, K.A., Sherwood, C.S., Turner, R.F.B., Haynes, C.A., 1996. Driving forces for DNA adsorption to silica in perchlorate solutions. *J. Colloid Interface Sci.* **181**, 635–644.

Mercier, P., Savoie, R., 1997. Interaction of DNA with silica particles: a vibrational spectroscopic study. *Biospectroscopy* **3**, 299–306.

Merkel, R., Nassoy, P., Leung, A., Ritchie, K., Evans, E., 1999. Energy landscapes of receptor-ligand bonds explored with dynamic force spectroscopy. *Nature* **397**, 50–53.

Moy, V.T., Florin, E.L., Gaub, H.E., 1994. Intermolecular forces and energies between ligands and receptors. *Science* **266**, 257–259.

Murashov, V.V., Leszczynski, J., 1999. Adsorption of the phosphate groups on silica hydroxyls: an ab initio study. *J. Phys. Chem. A* **103**, 1228–1238.

Omoike, A., Chorover, J., 2006. Adsorption to goethite of extracellular polymeric substances from *Bacillus subtilis*. *Geochim. Cosmochim. Acta* **70**, 827–838.

Omoike, A., Chorover, J., Kwon, K.D., Kubicki, J.D., 2004. Adhesion of bacterial exopolymers to alpha-FeOOH: inner-sphere complexation of phosphodiester groups. *Langmuir* **20**, 11108–11114.

Paizs, B., Suhai, S., 1998. Comparative study of BSSE correction methods at DFT and MP2 levels of theory. *J. Comput. Chem.* **19**, 575–584.

Papastavrou, G., Akari, S., 2000. Interaction forces between OH-groups in different solvents as observed by scanning force microscopy. *Colloid Surf. A-Physicochem. Eng. Asp.* **164**, 175–181.

Parks, G.A., 1965. The isoelectric points of solid oxides, solid hydroxides, and aqueous hydroxo complex systems. *Chem. Rev.* **65**, 177–198.

Patrick, D.L., Flanagan, J.F., Kohl, P., Lynden-Bell, R.M., 2003. Atomistic molecular dynamics Simulations of chemical force microscopy. *J. Am. Chem. Soc.* **125**, 6762–6773.

Persson, P., Nilsson, N., Sjoberg, S., 1996. Structure and bonding of orthophosphate ions at the iron oxide aqueous interface. *J. Colloid Interface Sci.* **177**, 263–275.

Reed, A.E., Curtiss, L.A., Weinhold, F., 1988. Intermolecular interactions from a natural bond orbital, donor–acceptor viewpoint. *Chem. Rev.* **88**, 899–926.

Reed, A.E., Weinhold, F., 1985. Natural localized molecular orbitals. *J. Chem. Phys.* **83**, 1736–1740.

Reed, A.E., Weinhold, F., Curtiss, L.A., Pochatko, D.J., 1986. Natural bond orbital analysis of molecular interactions—Theoretical studies of binary complexes of HF, H_2O, NH_3, N_2, O_2, F_2, CO, and CO_2 with HF, H_2O, and NH_3. *J. Chem. Phys.* **84**, 5687–5705.

Roddick-Lanzilotta, A.D., McQuillan, A.J., 1999. An in situ infrared spectroscopic investigation of lysine peptide and polylysine adsorption to TiO_2 from aqueous solutions. *J. Colloid Interface Sci.* **217**, 194–202.

Romanowski, G., Lorenz, M.G., Wackernagel, W., 1991. Adsorption of plasmid DNA to mineral surfaces and protection against DNase-I. *Appl. Environ. Microbiol.* **57**, 1057–1061.

Schwarz, U.D., 2003. A generalized analytical model for the elastic deformation of an adhesive contact between a sphere and a flat surface. *J. Colloid Interface Sci.* **261**, 99–106.

Schwenke, D.W., Truhlar, D.G., 1985. Systematic study of basis set superposition errors in the calculated interaction energy of two HF molecules. *J. Chem. Phys.* **82**, 2418–2426.

Spinner, S., 1956. Elastic moduli of glasses at elevated temperatures by a dynamic method. *J. Am. Ceram. Soc.* **39**, 113–118.

Stone, A.J., 1996. *The Theory of Intermolecular Forces*. Oxford University Press, New York.

Tomasi, J., Persico, M., 1994. Molecular-interactions in solution—an overview of methods based on continuous distributions of the solvent. *Chem. Rev.* **94**, 2027–2094.

Ulman, A., 1996. Formation and structure of self-assembled monolayers. *Chem. Rev.* **96**, 1533–1554.

van der Aa, B.C., Dufrene, Y.F., 2002. In situ characterization of bacterial extracellular polymeric substances by AFM. *Colloid Surf. B-Biointerfaces* **23**, 173–182.

Vandevivere, P., Kirchman, D.L., 1993. Attachment stimulates exopolysaccharide synthesis by a bacterium. *Appl. Environ. Microbiol.* **59**, 3280–3286.

Vorobyov, I., Yappert, M.C., DuPré, D.B., 2002. Hydrogen bonding in monomers and dimers of 2-aminoethanol. *J. Phys. Chem. A* **106**, 668–679.

Welch, S.A., Barker, W.W., Banfield, J.F., 1999. Microbial extracellular polysaccharides and plagioclase dissolution. *Geochim. Cosmochim. Acta* **63**, 1405–1419.

Whitchurch, C.B., Tolker-Nielsen, T., Ragas, P.C., Mattick, J.S., 2002. Extracellular DNA required for bacterial biofilm formation. *Science* **295**, 1487.

Wingender, J., Neu, T.R., Flemming, H.-C., 1999. What are bacterial extracellular polymeric substances? In: Wingender, J., Neu, T.R., Flemming, H.-C. (Eds.), *Microbial Extracellular Polymeric Substances: Characterization, Structure, and Function*. Springer, Berlin, pp. 1–19.

Wolfaardt, G.M., Lawrence, J.R., Headley, J.V., Robarts, R.D., Caldwell, D.E., 1994. Microbial exopolymers provide a mechanism for bioaccumulation of contaminants. *Microb. Ecol.* **27**, 279–291.

Wolfaardt, G.M., Lawrence, J.R., Korber, D.R., 1999. Function of EPS. In: Wingender, J., Neu, T.R., Flemming, H.-C. (Eds.), *Microbial Extracellular Polymeric Substances: Characterization, Structure, and Function*. Springer, New York, pp. 171–200.

Zhuravlev, L.T., 1987. Concentration of hydroxyl-groups on the surface of amorphous silicas. *Langmuir* **3**, 316–318.

Zhuravlev, L.T., 2000. The surface chemistry of amorphous silica. Zhuravlev model. *Colloid Surf. A-Physicochem. Eng. Asp.* **173**, 1–38.